Efficient Simulation of Time-Dependent Flows: Application to a Twin Screw Extruder

Janhavi S. Raut and Vijay M. Naik
Unilever Research India, Whitefield, Bangalore 560066, India

Thibauld R. Jongen
Unilever Research, 3133 AT Vlaardingen, The Netherlands

An efficient, versatile technique was developed for detailed simulation of flows in complex processing equipment with multiple moving parts. It uses a suitably modified finite-volume CFD simulation algorithm to deal with the problems posed by the relative motion of moving parts in processing equipment. A fixed grid is used to discretize the mass and momentum transport equations for the contents of the entire equipment volume. The motion of the solid moving parts within this domain is accounted for by assigning velocities to nodes of the grid representing the location of these parts at any moment of time. The technique was first validated for a single screw extruder by comparing the results predicted by conventional techniques involving body fitted mesh and a rotating frame of reference. Because of its inherent nonbody fitted mesh characteristics, the fixed grid method resulted in a rough, time-dependent boundary for the moving parts. The extent of error arising from this artifact was also evaluated. The benefits of this technique were demonstrated by simulating complex three-dimensional (3-D) flow in an industrially important processing equipment with multiple moving parts — an intermeshed counterrotating twin screw extruder. The time required for geometry generation and meshing using this approach was very small, and the relevant geometric parameters including those associated with the moving parts can be varied by simply modifying values in the analytical expressions used to define them. This technique does not require recreating or remeshing the entire geometry, thus making it easy to optimize the design of complex equipment via quick parametric studies.

Introduction

Computational fluid dynamics (CFD) simulations of equipment with multiple moving parts pose significant challenges. A number of equipment used in the processing industry, such as sigma mixers, Banbury mixers, planetary mixers, twin screw extruders, and so on, fall under this category. Flow field analysis of these equipment and, hence, their performance or design optimization is a complex task. Standard techniques for carrying out such analysis involve mesh deformation and regeneration which are computationally very expensive. Most CFD approaches usually adopt this body-conformal method to solve for the relative motion of the immersed boundaries. One standard example is the family of Arbitrary Lagrangian-Eulerian Deforming Mesh (ALE-DM) methods that have been developed with the aim to capture immersed moving boundaries within complex geometries (Hirt et al., 1974). In fully 3-D computations, this approach proves to be computationally very intensive and impracticable as soon as the amplitude of deformation becomes large. Alternative techniques involve breaking down the problem into tractable parts. For instance, a complex 3-D flow field can be solved by breaking down the problem into 2-D slices or decoupling the different flow types (such as rotation and translation in case of a twin screw extruder). The 3-D flow field is then recreated from these individual components.

Correspondence concerning this article should be addressed to J. S. Raut.

In recent years, fixed grid techniques (Glowinski et al., 1994; Tanguy et al., 1996; Shyy et al., 1996; Ye et al., 1999; Singh et al., 2000) are being introduced to simulate flows with immersed boundaries. In these methods, a fixed grid is used to discretize the mass and momentum transport equations for the contents of the entire equipment volume disregarding the immersed boundaries. The obvious advantage of these methods over the conventional body-conformal approach is that irrespective of the geometric complexity of the immersed boundaries, the computational mesh remains unchanged (Shyy et al., 1996). Thus, the initial meshing is greatly simplified. One way of accounting for the presence of the immersed boundaries and their motion within this domain is by assigning velocities to nodes of the grid representing the location of these boundaries at any instance of time. This approach is called the "forced cell" approach (Patankar, 1980), since the velocity vectors of the cells covered by the immersed boundaries are forced on to the velocities of those boundaries. In this article, we report our work on the forced cell approach, where a finite volume based CFD code (CFX-4 from AEA Technology) was extended to deal with the problems posed by the relative motion of moving parts in the processing equipment. The technique reported here is not new and is already available through commercial CFD packages with built-in features for the simulation of moving parts in the computational domain (for instance, the "Mesh Superposition Technique" in POLYFLOW or the "Moving Body Constraint" technique in FIDAP). However, one of the features of this work is that we present a simple way to modify a standard CFD package in order to extend its capabilities and deal with complex relative motion problems in an efficient manner. We demonstrate that this allows us to simulate flows with multiple boundaries moving with respect to each other very conveniently, thereby providing for a versatile and efficient tool for detailed simulation of flows in complex processing equipment. An additional benefit of the meshing simplicity associated with the method is that the whole simulation step can be included within a loop of an algorithm/program for design optimization of complex equipment.

This article begins with the development of a suitable forced cell formalism to solve the mass and momentum conservation equations with no-slip boundary conditions. Before applying the method to simulate complex equipment, its implementation is validated for the case of a single screw extruder. This is done by comparing the results obtained with those predicted using conventional techniques involving a body fitted mesh in a rotating frame of reference. The use of the forced cell approach, because of its inherent non-body fitted mesh characteristics, results into a rough time-dependent boundary for the moving parts. In order to evaluate the error arising out of this artifact, the validation is carried out in two steps. In the first step, the algorithm and its implementation is tested by having a body-fitted mesh for the single screw within the fixed grid implementation to eliminate the effect of the rough boundary. In the second step the extent of error arising out of the rough time-dependent boundary for the rotating screw is evaluated separately.

Having validated the method, we move on to demonstrate the power of this technique for the simulation of three-dimensional (3-D), time-dependent flows in complex processing equipment with multiple moving parts. For this purpose, the case of an intermeshed counter-rotating twin screw extruder has been simulated. We show that the instantaneous velocity vectors throughout the whole processing volume, including the complex screw gap geometries, can be obtained in a straightforward manner, without paying any special attention to meshing. Typical parameters used for the performance assessment of an extruder viz. its pumping efficiency, the degree of mixing/homogenization, product temperature, and so on can be readily probed by analysis of the velocity vectors. As an illustration, we have computed and presented estimates of "flow number" as defined in a later section, which can be used to quantify the flow type (viz. elongation vs. shear vs. rotational), and the degree of mixing achievable in the equipment.

Finally, a "real life" industrially relevant problem of soap plodding is presented. Conventional soap plodders are tangential twin screw extruders, which are used in the final stages of soap-bar processing. These extruders are expected to perform multiple functions of in-line homogenization, shear induced phase equilibration, plastication, and extrusion forming of the soap bar in its desired shape. In practice these plodders are neither ideal mixing, nor ideal pumping, devices. Some of the shortcomings of the conventional plodder arise from the extremely low energy efficiency of these machines ($< 5\%$). The excessive energy dissipated in the extruder causes structural breakdown of any shear sensitive products, as well as undesirable rise in its temperature leading to difficulties in downstream processing and deterioration of product attributes. The throughput of the conventional plodders is also very sensitive to the resistance offered by end fittings such as screens, perforated plates, dies, and so on, as well as to the rheology of the processed material. These factors impose enormous constraints on product formulations, which can be processed using this type of equipment. The soap plodder we have simulated is a recent innovation called Low Energy Plodder (LEP) employing intermeshed counter-rotating twin screws as against the tangential screws fitted in the barrel of a conventional plodder. These LEPs are expected to deliver relatively pressure gradient independent flow (positive displacement pumping action) owing to axially and radially closed C-shaped cavities formed in the discharge zone of the screws. They would, hence, deliver higher throughput at a given RPM and consume less energy per unit of extruded mass. In the LEP assembly simulated here we have included a stationary pressure plate followed by a convergent cone and a die, all fitted at the discharge end of the extruder. Although a full study of the performance of the plodder falls outside the scope of this article, it is shown that such an extremely complex piece of equipment can be efficiently simulated with the proposed methodology. Despite the inaccuracies that might arise out of the non-body fitted mesh in our approach, its inherent meshing simplicity makes it a perfect tool for design optimization, at least to get a maiden-cut on the design parameters. The more computationally intense methods may then be used to get further refinement on the design.

Numerical Scheme

The flow of an incompressible fluid in any space domain $\Omega(t)$ is governed by the following equations for mass and mo-

mentum conservation

$$\left.\begin{aligned} \nabla\cdot\bar{u} &= 0 \\ \rho\frac{\partial}{\partial t}\bar{u} + \rho\bar{u}\cdot\nabla\bar{u} + \nabla\cdot\bar{\bar{\tau}} + \nabla P &= 0 \end{aligned}\right\} \tag{1}$$

where $\bar{u}$ is the velocity vector, ρ is the fluid density, and P is the pressure. The stress tensor $\bar{\bar{\tau}}$ can be related to the velocity field using an appropriate constitutive equation for the fluid under consideration. The simplest constitutive model is that for a Newtonian fluid given by

$$\tau_{ij} = -2\mu S_{ij} \tag{2}$$

where μ is the constant fluid dynamic viscosity. We employ this constitutive model in the initial part of our work to illustrate the methodology. In the final section we use a more complex Herschel-Bulkley model as described later. The strain rate tensor S_{ij} and the rotation rate tensor W_{ij} for the fluid elements are defined by

$$\begin{aligned} S_{ij} &= \frac{1}{2}\left(\frac{\partial}{\partial x_j}u_i + \frac{\partial}{\partial x_i}u_j\right) \\ W_{ij} &= \frac{1}{2}\left(\frac{\partial}{\partial x_j}u_i - \frac{\partial}{\partial x_i}u_j\right) \end{aligned} \tag{3}$$

The velocity of a point $\bar{x}$ on any moving solid body (such as screws, mixing blades, and so on, in a processing equipment) can be described by the equation

$$\bar{u}_{\text{body}}(\bar{x}) = \bar{\omega}_{\text{body}} \times (\bar{x} - \bar{x}_c) + \bar{u}_c \tag{4}$$

where $\bar{u}_{\text{body}}(\bar{x})$ is the velocity at a point $\bar{x}$ on the solid body, resulting from the rotation and translation of the body. $\bar{\omega}_{\text{body}}$ is the angular velocity of the moving body about its rotational axis located at $\bar{x}_c$, in a plane normal to the axis and passing through $\bar{x}$. $\bar{u}_c$ is translational velocity of the rotational axis of the body.

Consider equipment with a moving solid body mounted within it (c.f., Figure 1a). Let $\Omega_{\text{body}}(t)$ represent the space domain occupied by the solid body within the equipment. Let the domain occupied by the fluid be given by $\Omega(t)$. The entire equipment domain Ω_T thus comprises $\Omega_{\text{body}}(t)$ and $\Omega(t)$, that is, $\Omega_T = \Omega(t) \cup \Omega_{\text{body}}(t)$. To obtain the flow field inside this equipment, the equations of mass and momentum conservation (Eq. 1) can be discretized and solved for this fluid domain $\Omega(t)$. However, as the solid body moves, the domains occupied by both the solid body $\Omega_{\text{body}}(t)$, as well as the fluid $\Omega(t)$ within the equipment volume, change with time. This poses significant problems since the computational grid on which the mass and momentum conservation equations are solved within the fluid domain, $\Omega(t)$ also has to be distorted and/or remeshed with time. In order to avoid this costly re-meshing step we made use of a simplifying relationship. In case of solid bodies, where no-slip boundary conditions are applicable at the interface between the solid body and the fluid, the fluid velocity field $\bar{u}(\bar{x})$ for $\Omega(t)$ can be extended to

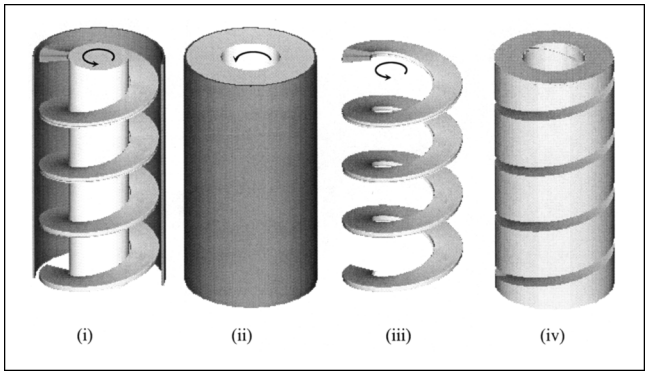

Figure 1a. Single screw extruder:(i) Extruder assembly; definition of different space domains (ii) Ω_T, (iii) $\Omega_{\text{body}}(t)$, and (iv) $\Omega(t)$.

space $\bar{x} \in \Omega_{\text{body}}(t)$ for defining a divergence-free field in the entire equipment domain, Ω_T. Basically, the no-slip boundary condition is transformed into a constraint on the fluid velocity within the solid body, and for any $\bar{x} \in \Omega_{\text{body}}(t)$, $\bar{u}(\bar{x}) = \bar{u}_{\text{body}}(\bar{x})$, as defined by Eq. 4. Consequently, the equations of motion for the fluid are solved over the entire equipment domain Ω_T, which does not change with time. Immense advantage is derived out of defining this time invariant domain Ω_T, since it has to be meshed only once (Duchanoy and Jongen, 2003). The set of equations for $\bar{u}$ are now

$$\begin{aligned} \nabla\cdot\bar{u} &= 0 && \text{for} \quad \bar{x} \in \Omega_T \\ \rho\frac{\partial}{\partial t}\bar{u} + \rho\bar{u}\cdot\nabla\bar{u} + \nabla\cdot\bar{\bar{\tau}} + \nabla P &= 0 && \text{for} \quad \bar{x} \in \Omega(t) \\ \bar{u}(\bar{x}) &= \bar{\omega}_{\text{body}} \times (\bar{x} - \bar{x}_c) + \bar{u}_c && \text{for} \quad \bar{x} \in \Omega_{\text{body}}(t) \end{aligned} \tag{5}$$

The finite volume discretization of Eq. 5 in the "real" fluid flow domain $\Omega(t)$ follows the classical second-order cell-centered finite volume arrangement, with a SIMPLE type pressure-correction (Van Doormal and Raithby, 1984) algorithm using Rhie-Chow interpolation (Rhie and Chow, 1983). In this case, the governing transport equations for each velocity component can be rewritten under the generic scalar advection-diffusion equation of the form

$$\rho\left(\frac{\partial}{\partial t}\Phi + \bar{u}\cdot\nabla(\Phi - \mu_\Phi\nabla\Phi)\right) = S_\Phi \tag{6}$$

The standard finite volume discretization of Eq. 6 on a structured grid covering the total domain Ω_T leads to the following set of algebraic equations

$$\sum_{nb \in NB} A_{nb}(\Phi_{ijk} - \Phi_{nb}) = S_\Phi^c + S_\Phi^l \Phi_{ijk} \tag{7}$$

for all (i,j,k) within the grid G. The set of points NB spans all the neighboring nodes involved in the spatial discretization of the partial differential equation (Eq. 6). The source term S_Φ^c contains the values of the unknown at the previous time step, as well as the constant term of S_Φ. The discretiza-

tion of the scalar transport equation is done by standard techniques, which are described in the literature (Patankar, 1980).

The grid variable Φ_{ijk} is defined on the whole domain Ω_T, and satisfies Eq. 6 on $\Omega(t)$. In order to impose the conditions (Eq. 4) at grid nodes covered by the solid body, Ω_{body} an auxiliary function α_{ijk} is defined on the grid G

$$\alpha_{ijk} = \begin{cases} 0 & \text{for} \quad x_{ijk} \in \Omega(t) \\ 1 & \text{for} \quad x_{ijk} \in \Omega_{\text{body}}(t) \end{cases} \tag{8}$$

where x_{ijk} denotes the co-ordinates of the center of the control volume (i,j,k). The coefficients of the discrete transport equation (Eq. 7) are then modified as follows

$$\begin{aligned} A^*_{nb} &= A_{nb}\left(1 - \alpha_{ijk}\right) \\ S^{c*}_{\Phi} &= S^c_{\Phi}\left(1 - \alpha_{ijk}\right) - \alpha_{ijk}\tilde{\Phi}_{ijk} \\ S^{l*}_{\Phi} &= S^l_{\Phi}\left(1 - \alpha_{ijk}\right) + \alpha_{ijk} \end{aligned} \tag{9}$$

This leaves the original values of the discretization coefficients unchanged for the points in the fluid domain $\Omega(t)$, whereas for the points in the moving bodies, the grid variable Φ_{ijk} will be equal to the prescribed value $\tilde{\Phi}_{ijk}$ given by Eq. 4 for each component of the velocity. Thus, following this scheme, the discrete counterpart of Eq. 5 will be fulfilled, with Eq. 5b satisfied in $\Omega(t)$, Eq. 5c imposed in $\Omega_{\text{body}}(t)$, and the incompressibility constraint 5a valid in Ω_T. This is valid irrespective of the choice of rheological constitutive equation for the fluid domain. Note that the same approach can be utilized to assign specific material properties like density, specific heat, heat-transfer co-efficient and so on to the moving bodies. Thus, heat-transfer calculations, and so on can also be incorporated within the same framework.

Validation for a Single-Screw Extruder

The method was first implemented for the simulation of metering zone of a single screw extruder as shown in Figure 1a(i). The purpose of this exercise was to validate the method by comparing it with a conventional technique using a body fitted mesh and a rotating frame of reference. The equipment comprises a stationary barrel and a screw rotating within it with angular speed ω. The equipment geometrical parameters were set as follows: assembly length = 400 mm, barrel radius = 110 mm, screw radius = 100 mm, shaft radius = 50 mm, pitch = 100 mm, flight thickness = 10 mm at the land of the screw. A Newtonian fluid was used with viscosity $\mu = 1.08$ Pa·s.

For the "Forced Cell" (henceforth, referred to as FC) implementation, the three space domains Ω_T, $\Omega_{\text{body}}(t)$, and $\Omega(t)$, were visualized and defined as shown in Figures 1a(ii), 1a(iii), and 1a(iv), respectively. The total equipment domain Ω_T was visualized as a cylindrical annulus. Its two curved surfaces were bound by (a) the inner stationary skin of the barrel wall and (b) by the skin of an imaginary rotating hollow shaft mounted inside the barrel. No slip boundary conditions were applied at both the curved wall surfaces. The top and bottom flat surfaces were defined as the inlet/outlet planes. The rotating screw was visualized as a shaftless helical auger with space domain $\Omega_{\text{body}}(t)$ which rotated at the same angular velocity as that of the inner cylindrical boundary of Ω_T. The fluid domain $\Omega(t)$ was given by the difference $\Omega_T - \Omega_{\text{body}}(t)$. The clearance region between the land of the screw and the barrel wall has not been shown in the Figure 1a(iv), which depicts $\Omega(t)$, merely to simplify the diagram. The screw was made to rotate about the z-axis. The resulting velocity components of the cells covered by the screw at any instant of time were obtained using Eq. 4. $\bar{u}_c$ was set to 0, since the screw rotated about a stationary axis. As the screw rotated during the course of the simulation, the location of $\Omega_{\text{body}}(t)$ at any time t was obtained using the analytical expression

$$\theta = \frac{z}{\text{pitch}} \times 2\pi + \omega \times t \tag{10}$$

where θ was the angle made by the centerline of the flight with a reference axis (x) (*c.f.* Figure 1b). The first term on the righthand of Eq. 10 gave the change in θ as we moved along the shaft (function of height z) and the second term gave its time evolution as the screw rotated with an angular speed ω. The flight thickness could be varied by appropriately assigning the angular span $\Delta\theta$ around the centerline, in a plane perpendicular to the z-axis. The equations were plugged into the User-Fortran subroutines of CFX-4 to simulate the problem. In the CFX implementation of the "Forced Cell" approach, the exact location of the boundary of the moving part is known up to one mesh cell thickness as partial coverage of the cell by the body is not taken into account. This results in a loss of accuracy close to the boundary of the moving body, which acts effectively as a (time-dependent) rough surface. Use of sufficiently small mesh elements can minimize this effect. The partial coverage of a cell by a moving body in the case of a single screw extruder results in a "spiral-staircase" like structure for the screw. A smooth screw surface can be generated by using a mesh that is not aligned with the screw (Z) axis, but twisted around the axis in sync with the screw pitch. In the reported simulations of the single screw extruder, both a twisted grid and a straight grid (*c.f.* Figure 1b) were used to isolate the effect of the rough screw

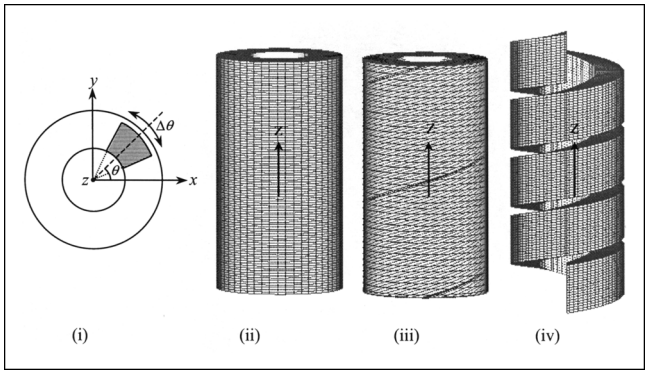

Figure 1b. Single screw extruder: (i) Coordinate frame, (ii) straight mesh for Ω_T of FC method, (iii) twisted mesh for Ω_T of FC method, and (iv) mesh for conventional method.

surface on the results. For the conventional approach, the computational domain was the free space $\Omega(t)$ in the screw-barrel assembly, occupied by the fluid. The entire problem is solved using a rotational frame of reference (angular speed ω). The extruder barrel wall was assigned a negative angular velocity ($-\omega$) w.r.t. the frame of reference. The computational domain $\Omega(t)$ was thus stationary w.r.t. the frame of reference. For discretization of the computational domain, a comparable number of elements were employed for both the approaches. A total of 216,320 elements were used in the case of the RFR approach, while, for the FC approach, 230,400 elements were used.

Simulations were carried out for the case of an externally imposed flow through the equipment from top to bottom. Identical mass-flow rates and rotational speed ω of the screws were used as the basis of comparison between the two methods. Appropriate normal velocities were assigned at the inlet zones (taking into account the flight location in case of the FC method) for the two methods such that the mass-flow rates were the same. Fully developed flow was assumed at the outlet zone. Results were compared at different sections of the geometries (x-y and x-z) and are reported below. The x-y section was taken at the center of the extruder and the x-z section was taken at the $y = 0$ plane. The contours of the x, y, and z components of the velocity are compared at x-y (*c.f.* Figure 2a) and x-z (*c.f.* Figure 2b) planes. The results are presented for a screw rotated anti-clockwise at a speed of 13.37 rpm and an impressed throughput rate of 0.1637 kg/s. A quantitative comparison is also made by extracting data along a line parallel to the central axis at radius $R = 105$ mm at the central x-z plane and a circular line at $R = 95$ mm on the central x-y plane. We shall be referring to these two lines as the Z-line and the R-line, respectively, in the rest of the article. The line data is plotted in Figures 3a and 3b. In the x-z sections, as well as the Z-line plots, we have ignored about one pitch length distance from the two ends. This was done

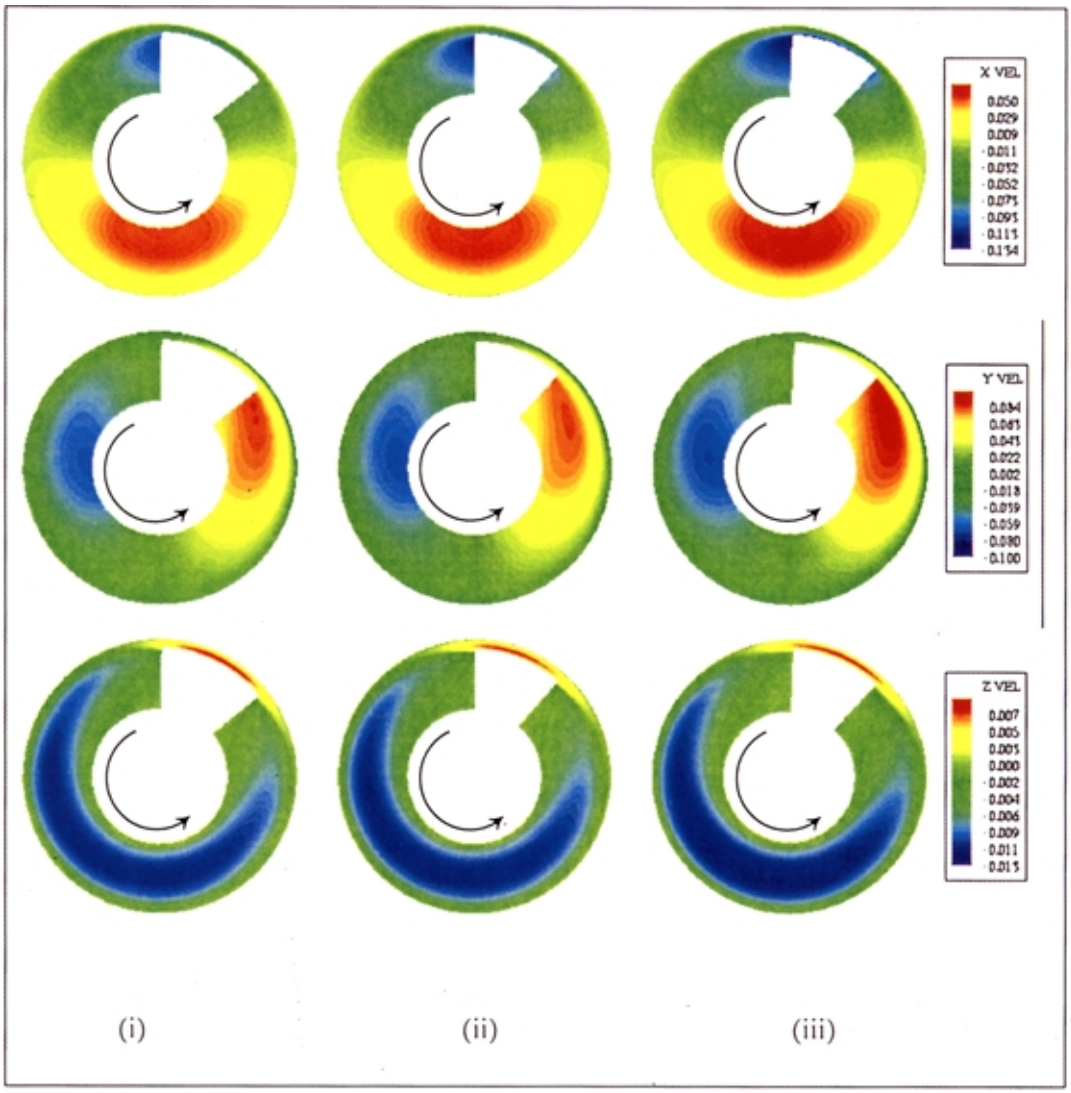

Figure 2a. (i) Comparison of the X-, Y-, and Z-velocity components at the central x-y slice for FC method with rough screw surface; (ii) FC method with smooth screw surface; and (iii) conventional method.

The legend indicates the velocity values in m/s.

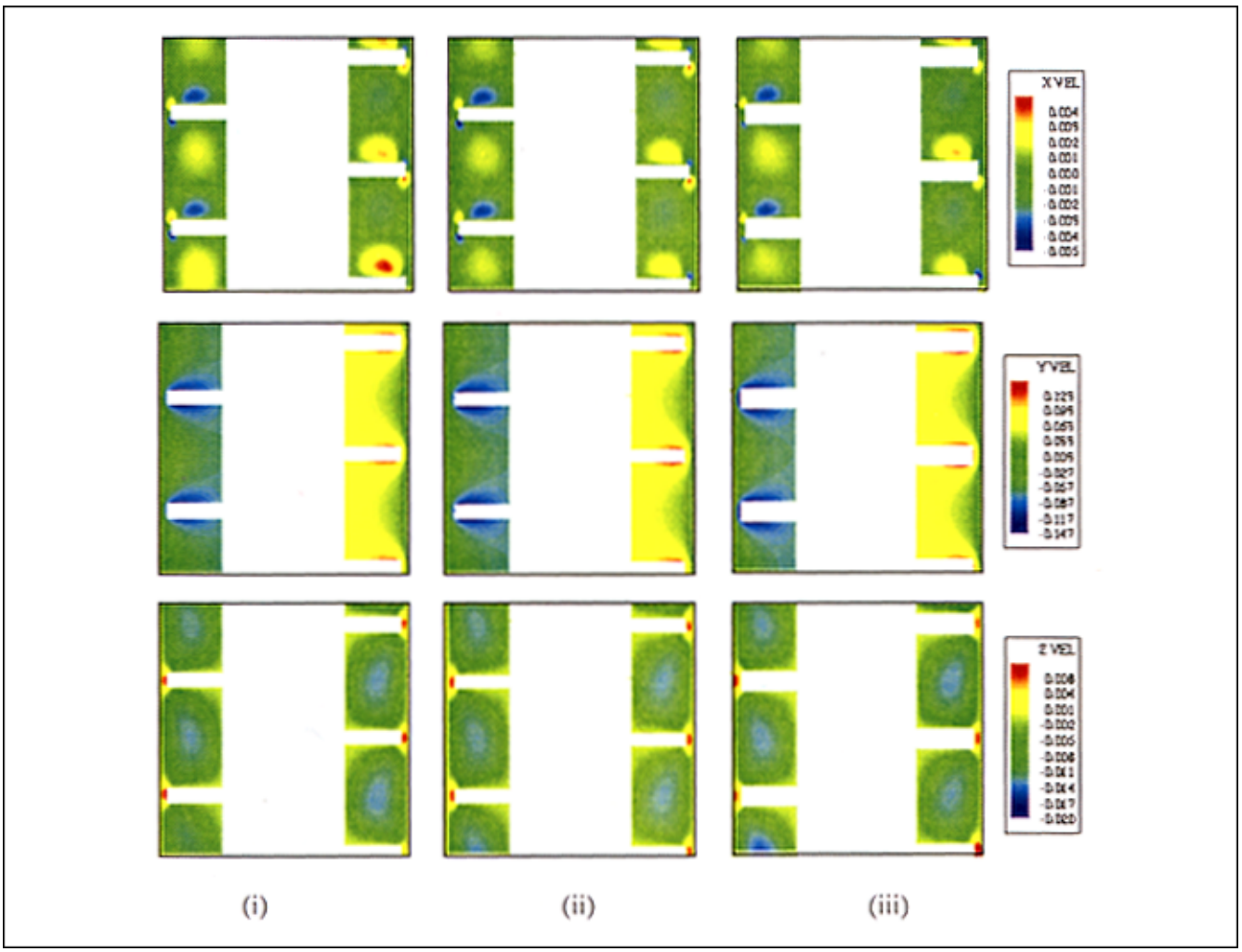

Figure 2b. (i) Comparison of the *X*-, *Y*-, and *Z*-velocity contours at the central *x*-*z* slice for FC method with rough screw surface; (ii) FC method with smooth screw surface; and (iii) conventional method.

The legend indicates the velocity values in m/s.

in order to eliminate the end effects arising out of the different inlet/outlet regions in the two approaches. In case of the "forced cell" approach, the inlet/outlet zones are at a constant z-value, while, for the conventional case, the inlet/outlet zones are perpendicular to the down channel direction of the helix. The agreement between the FC and the conventional approach is seen to be very good. There is also very good agreement between the two mesh types in the "forced cell" approach indicating that the effect of the rough surfaces is not felt much beyond the immediate cells and dies out rather quickly. This illustrates that, at least as far as the velocity components are concerned, the FC approach irrespective of the choice of the grid shows excellent agreement with the conventional approach. In Figure 4 and Figure 5 we have compared the pressure drop contours at the two sections. A reference pressure (P_{ref}) at ($x = 105$ mm, $y = 0$, $z = 0$) was subtracted from the actual pressure values. No explicit constraints were imposed on the pressure within the moving/stationary parts in the FC framework; hence, a comparison of the pressure contours is a more stringent test of the FC approach. As seen in the two figures, the pressure contours, as well as the quantitative plots obtained using the conventional approach and the FC approach for both the mesh types, agree very well with each other. This shows that the pressure values do evolve correctly in accordance with the flow imposed on the solid parts. The pressure contours obtained using FC with a rough surface shows the effect of the rough surface, as seen in Figure 4a(i) near the screw blade, but this effect dies out very quickly.

For Newtonian flow in a single-screw extruder, the throughput Q is given by the expression (Rowell and Finlayson, 1928)

$$Q = \frac{1}{2} UWBF_D - \frac{WB^3}{12\mu} \frac{\Delta P}{\Delta Z'} F_P \tag{11}$$

where W is the channel width, B is the channel height, F_D and F_P are the shape factors that express the effects of the flight walls, and $\Delta P/\Delta Z'$ is the pressure drop per unit length of the extruder channel. The down channel velocity U is given by $U = \pi DN\cos\theta$, where D is the outer screw diameter, θ is the pitch angle, and N is the rotational speed. Equation 11 is

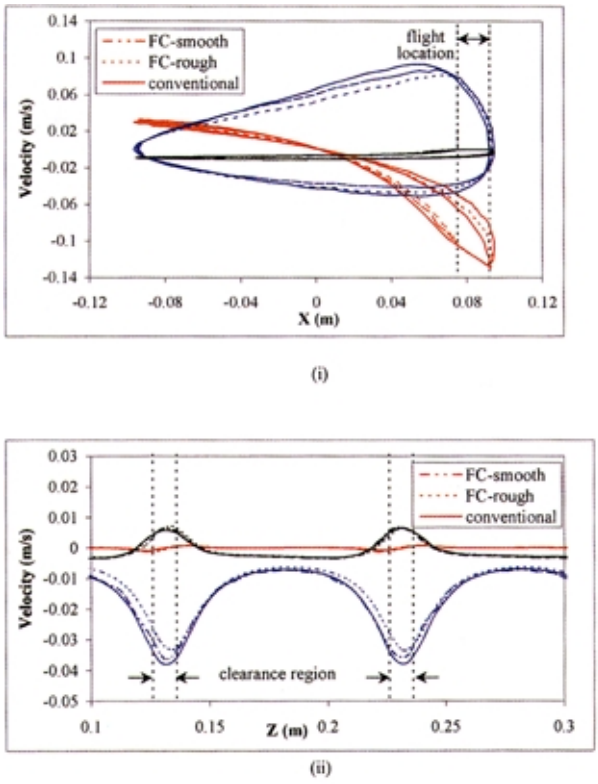

Figure 3. Comparison of the *X*-(red), *Y*-(blue), and *Z*-(black) velocity components on the (i) *R*-line and (ii) *Z*-line for the FC and conventional method.

the basis of the "screw characteristic curve" representation that relates throughput Q to the pressure gradient $\Delta P/\Delta Z'$ at specified screw speed N. In Figure 6 we have plotted Q vs. $\Delta P/\Delta Z'$ plot for the FC (with the two grids) and conventional approaches. Since the inlet/outlet planes are different in the two cases, the pressure drop was measured in the central section of the extruder leaving out a distance of one pitch length from the two ends to eliminate end effects. Thus, the pressure gradient reported is an average across two pitch lengths of screw. As shown in the figure, the "screw characteristic curves" obtained using the two approaches are linear, as is expected for a Newtonian fluid and in good agreement with each other.

Thus, a thorough validation of the FC technique for the case of a single screw extruder was accomplished. The presence of the rough surface in the case of the forced cell approach did not appear to significantly influence the velocity-components or the pressure drop across the fluid volume. We must caution, however, that the analysis was done for a Newtonian fluid; and the results might be different for a non-Newtonian fluid, where the rough edges may play a more or less significant role in altering the flow field. A pseudoplastic fluid, for instance, trapped inside the rough edges would act like a solid mass and, hence, tend to smooth out the effects on the fluid flow. A dilatant fluid on the other hand could induce some sort of wall slippage. The effect on a non-Newtonian fluid would have to be explored further. The CPU time required on a SGI R10K processor for a 1 iteration step for the conventional simulation was ~124 s, while, for the FC method, it was ~138 s. Both the FC and conventional techniques converged in about 550 iteration steps. Although the FC method took about 10% higher CPU time for the case of a single screw extruder, this would not hold true for complex equipment. In addition to the geometry generation and meshing time being considerably lower, it is expected that the FC implementation would also afford significant savings in the computational time, especially in comparison to the mesh deformation and regeneration technique.

Intermeshed Counter-Rotating Twin Screw Extruder

Twin-screw extruders have been of great interest in the processing of complex materials across a range of industries (Janssen, 1978; White, 1991). Among the different classes of twin screw extruders, the intermeshed counter-rotating twin screw extruders are known for better pumping efficiencies combined with low shearing action and narrower residence time distributions (Shon et al., 1999). This is a consequence of the axially and radially closed C-cavities formed in an intermeshed counter-rotating twin screw extruder, which pro-

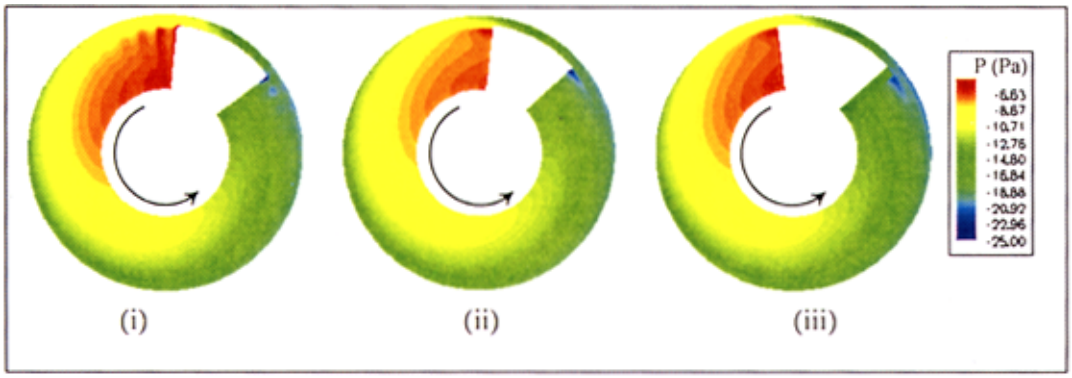

Figure 4a. (i) Comparison of the pressure contours at the central *x*-*y* slice for FC method with rough screw surface; (ii) FC method with smooth screw surface; and (iii) conventional method.

The legend indicates the pressure values in Pa.

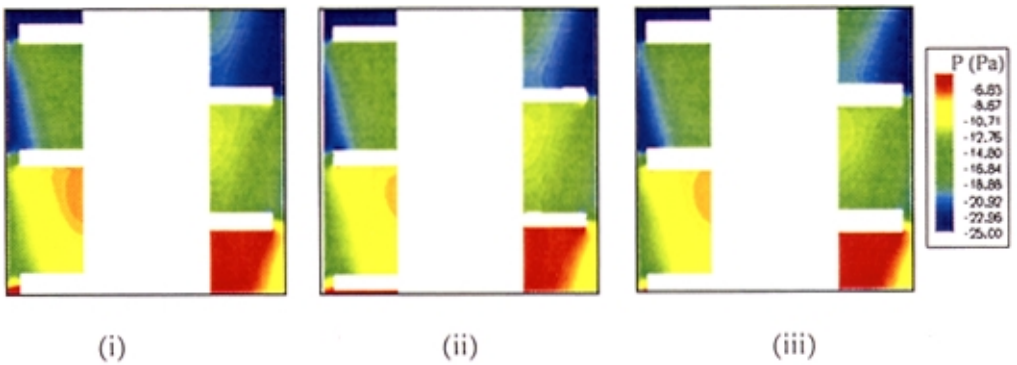

Figure 4b. (i) Comparison of the pressure contours at the central *x*-*z* slice for FC method with rough screw surface; (ii) FC method with smooth screw surface; and (iii) conventional method.

gressively move in the axial direction with the passage of time. This geometrical constraint also makes the nearly positive displacement type flow in an intermeshed counter-rotating less sensitive to the die characteristics. An insight into the transient flow field of these extruders would be useful for assessing and optimizing their design and performance characteristics (such as torque on the screw, power consumption, residence time distribution, throughput vs. pressure drop characteristics, extent of shear degradation/mixing, and so on). Techniques like the boundary element method (Rios et al., 1998), and solving by selecting a number of sequential geometries to represent a complete rotational cycle (Yang and Manas-Zloczower, 1992; Ishikawa et al., 2001) have been reported in literature for studying flow in these extruders. In recent times, the mesh superposition technique of POLYFLOW has been used (Avalosse et al., 2002) to simulate 3-D flow in twin screw extruders. We present complete 3-D transient simulations of flow in an intermeshed counter-rotating twin screw extruder using the forced cell approach.

The geometry of the twin screw extruder considered in this article is shown in Figure 7. Such extruders are recently being introduced for industrial processing of soaps. They are called Low Energy Plodders (LEP) (Chokappa and Naik, 1995). The equipment consists of a barrel with a "figure-of-8" cross-section in which two rotating intermeshed screws are placed. The screw geometry is not uniform along the length of the machine. As seen in Figure 7, the flight thickness and the shaft diameter vary along the length of the extruder. The extruder can be conceptually divided into 3 zones viz.: (i) feed, (ii) transition, and (iii) metering or discharge. The various geometry parameters are given in Table 1. The screws are more open near the feed zone since the feed is pelletized, and they progressively close near the metering zone resulting in axially and radially closed C-cavities. We have simulated a com-

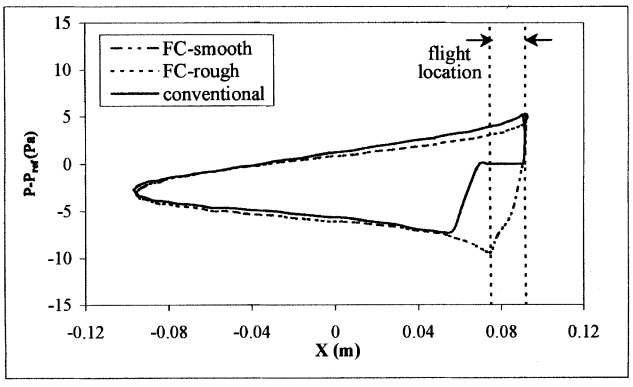

Figure 5. Comparison of the pressure values at the (i) *R*-line and (ii) *Z*-line for the FC and conventional method.

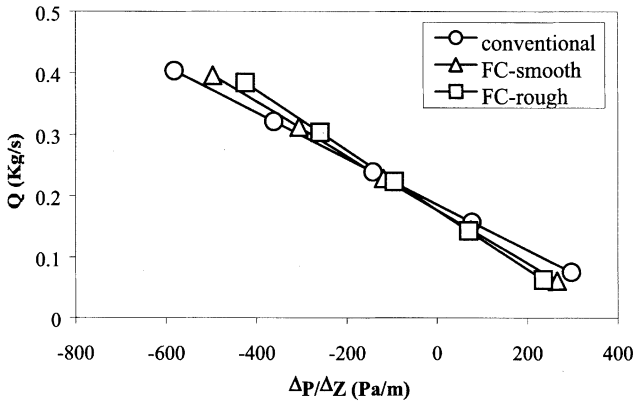

Figure 6. Screw characteristic curves for the FC (with rough and smooth screw surface) and conventional method.

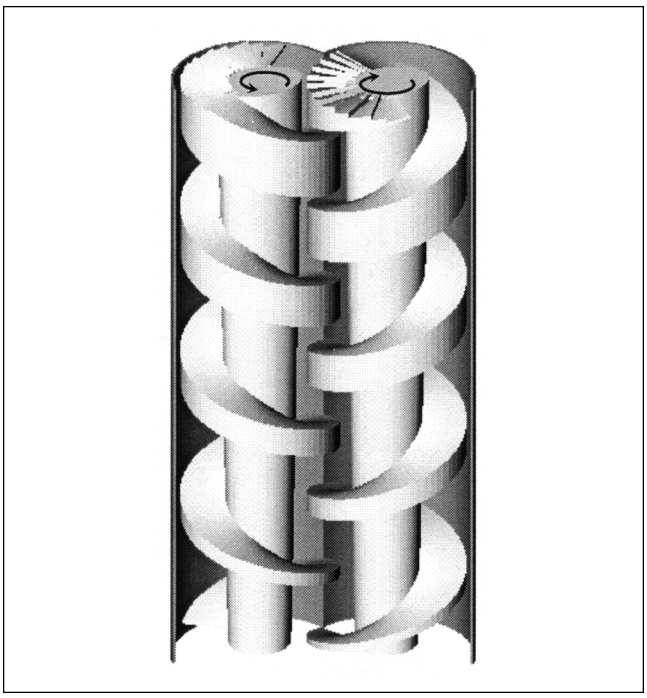

Figure 7. Twin screw extruder: extruder assembly.

pletely flooded situation across the entire length of the screw. The analytical expressions used for the screw geometry and its rotation are given below

$$\theta_1 = \frac{z}{\text{pitch}} \times 2\pi + \omega \times t \tag{12a}$$

$$\theta_2 = -\frac{z}{\text{pitch}} \times 2\pi + \omega \times t \tag{12b}$$

In Eq. 12, θ_1 and θ_2 are the angles made by the centerline of the two screws with a reference axis (x). Screw 1 is right-handed and rotates in the clockwise direction, while screw 2 is lefthanded and rotates in the anti-clockwise in order to pump material from the feed end to the discharge end. θ_1, θ_2, and ω are positive when measured in anticlockwise direction w.r.t. x-axis. The angular span $\Delta\theta$ of the screw domain

Table 1. Twin Screw Extruder: Geometry and Discretization of the Geometry

Geometric Dimensions	
Barrel and screw length	$L_s = 1470$ mm
Barrel radius	$R_b = 200$ mm
Shaft radius	$R_{sh} = 37.5$–50 mm From inlet to outlet
Screw radius	$D_s = 190$ mm
Screw pitch:	$P_s = 38$ mm
Flight thickness at $R_s = 190$ mm:	
Feed Zone: (400 mm length)	$T_f = 30$ mm
Transition zone: (500 mm length)	$T_f = 30$–160 mm
Discharge zone: (570 mm length)	$T_f = 160$ mm
Discretization of Computational Domain	
FC: For each cylindrical shell $r \times t \times z$	600,000 elements
Radial	40
Circumferential	100
Length	150

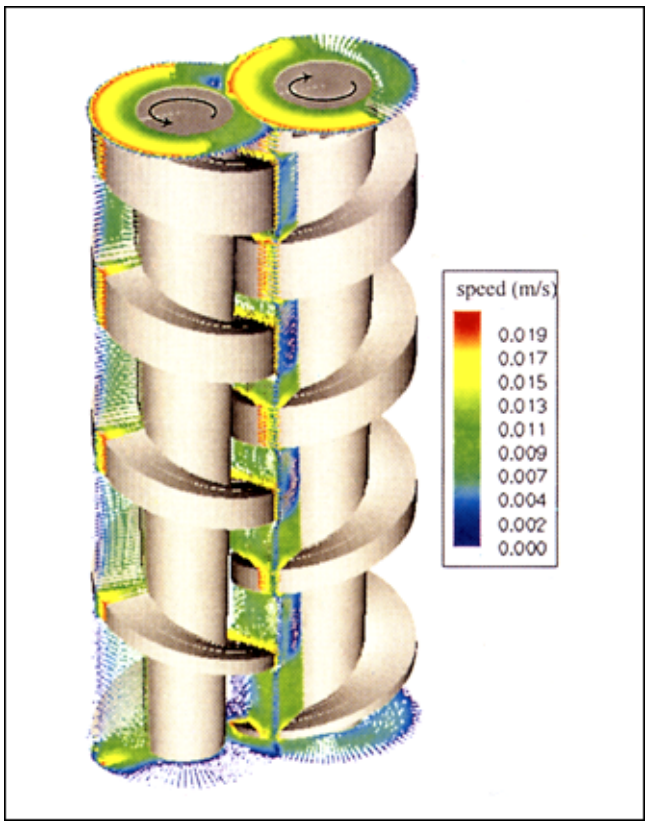

Figure 8. Velocity vectors for the twin screw extruder using the FC method.

The colors indicate the speed values in m/s.

varies as a function of z depending on the flight thickness. The three computational space domains (Ω_T, $\Omega_{\text{body}}(t)$, and $\Omega(t)$) for the twin screw extruder were defined in the same way as that for the single screw extruder. The discretization of the equipment domain is given in Table 1. A total of 1,200,000 elements were used. The CPU time required for the simulation of the twin screw extruder on a SGI R10K processor was 142 s for a single iteration. A time step about 1/100 of the time of one revolution took $\sim$100 iterations to converge. Thus, one revolution of the screws would require $\sim$15 days of CPU time. Comparison with other techniques is not available.

The instantaneous velocity vectors obtained for the twin screw extruder in Figure 7 are shown in Figure 8 for a few representative slices through the flow domain. The leakage flows in a twin screw extruder control the working of the twin screw extruder to a great extent. The drag and pressure flows are restricted to the C-chambers, and their influence on the throughput of the extruder is only via the leakage flows. The leakage flows are normally not easy to calculate given the complicated geometry of the various gaps. Janssen et al. have obtained analytical expressions for the flow of Newtonian fluids through the calender and flight gaps. However, for the flow description through a tetrahedral gap between the screw flights, only empirical expressions are available to date. The various leakage flows have been magnified and are shown in Figure 9. The calender leakage is shown in Figure 9(i). The velocity profile is qualitatively in agreement with Janssen's

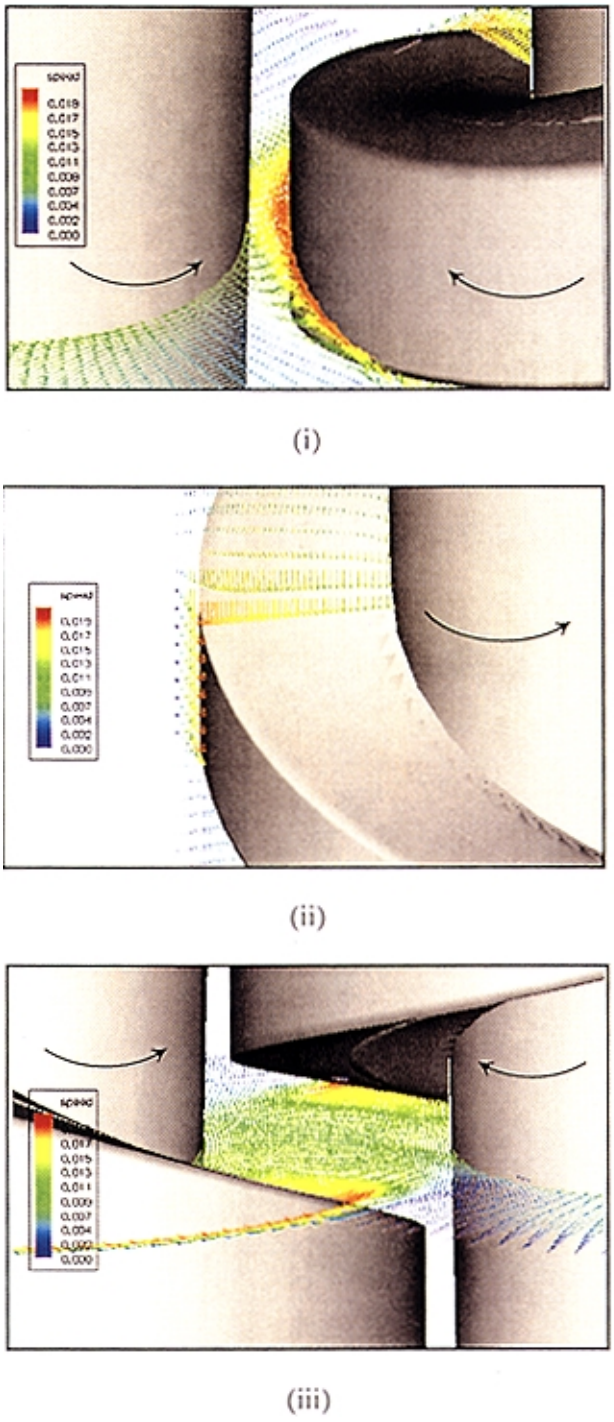

Figure 9. Velocity vectors through different gaps in an intermeshed counterrotating twin screw extruder: (i) calender gap, (ii) flight gap, and (iii) tetrahedral gap.

The legend indicates the speed values in m/s.

expression of combined pressure (parabolic) and shear flow (linear) in the same direction (Speur et al., 1987). Note that the pressure gradient across the gap is fairly low due to the large gap sizes specified in our illustrative screw geometry. The flight leakage flows (*c.f.* Figure 9(ii)) is also due to the

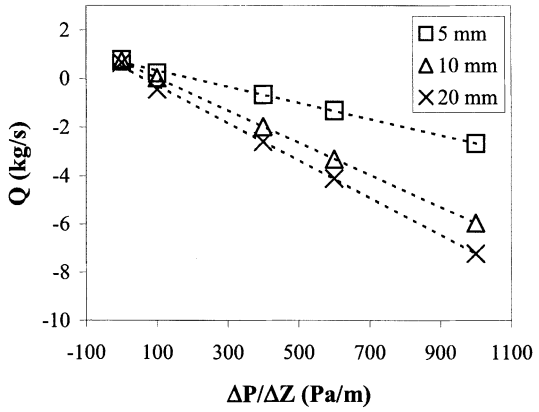

Figure 10. Screw characteristics for the twin screw extruder as a function of (flight) clearance gaps at the land of the screw.

combined effects of drag and pressure over the land of the screw. However, in this case the drag flow and the pressure flow act are in opposite directions. The pressure leakage flows in the tetrahedron gap (*c.f.* Figure 9(iii)) between the flanks of the screws is seen to have a rather complex velocity profile. The simulation results indicate that all of the three leakage flows discussed above increase with increasing axial pressure gradient.

The intermeshed counter-rotating twin screw extruder, with closed channels, acts like a positive displacement pump delivering pressure independent flow. In Figure 10 we have plotted the "screw characteristic curve" for different values of

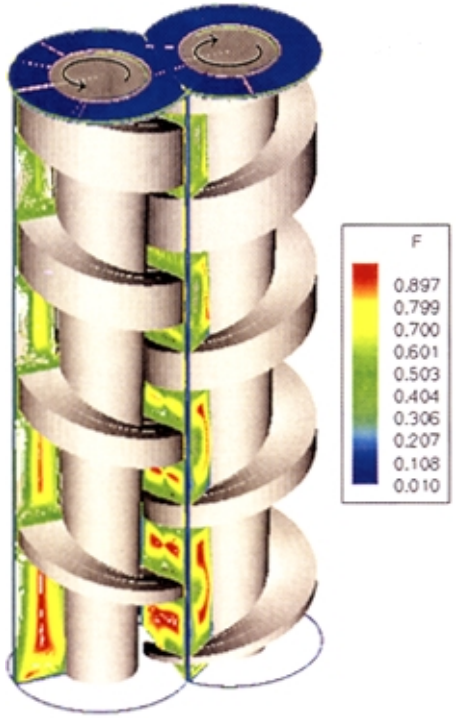

Figure 11a. Flow number (*F*), contours using the forced cell approach through a twin screw extruder.

clearances between the land of the screw and the barrel. Since the flight gap has been manipulated by changing the screw radius ($R_s = 180$ mm, 190 mm, 195 mm), the calender gap also gets altered simultaneously for the three simulation cases presented in Figure 10. As is apparent, the flow characteristics become increasingly horizontal (pressure independent) as the clearance is reduced thus indicating that the flow becomes increasingly independent of the die characteristic as the clearance gaps are reduced.

The knowledge of the position and time-dependent velocity vectors enables us to derive parameters that characterize the type and extent of deformation taking place in any equipment. Flow patterns can be broadly classified into three deformation types: elongational, shear, and rotational. One parameter that has been used in the literature (Li and Manas-Zloczower, 1994; Wilson et al., 1995; Gramann et al., 1995) to identify the type of flow is the flow number. The flow number F is defined as

$$F = \frac{s}{s + \omega} \tag{13}$$

where $s = \text{trace}(\bar{\bar{S}}^2)$ and $\omega = \text{trace}(\bar{\bar{W}}^2)$. S and W are the strain rate and rotation rate tensors defined in the second section. Thus, $F \in [0,1]$, and takes the following values in particular: $F = 0$ for pure rotational flow, $F = 1$ for pure elongational flow, and $F = 0.5$ for pure shear flow. Note that the above criteria are strictly valid for planar flows only, and generalizations to fully 3-D flows are ambiguous and nontrivial (Jongen, 2000). However, these criteria have been used in flow classification in 3-D flows because of their simplicity. We have examined the flow numbers at different regions within the extruder to investigate prevailing flow types. In Figure 11a, we have plotted the instantaneous distribution of F at the central x-y and x-z planes. For the screw geometry simulated, the intermesh gap is progressively reduced as we move from the feeding zone to the discharge zone. The effect of this on the flow behavior is apparent from the figure. In the feeding zone where the gaps are relatively large, the flow has a larger elongational component in the tetrahedral gaps where the fluid is drawn in through the narrow regions, as well as at the center of the C-chambers. On the other hand, in the fully intermeshed discharge region, the flow in the C-

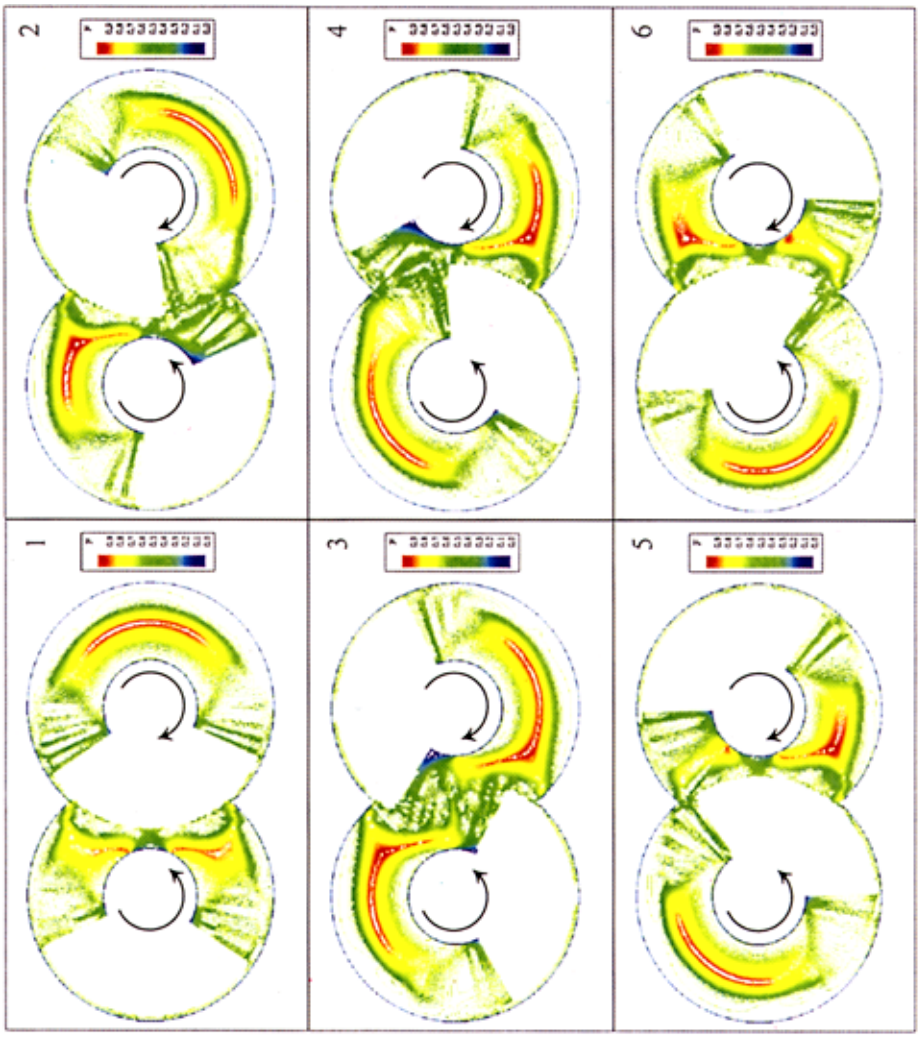

Figure 11b. Sequence of instantaneous distributions of the Flow Number (F) at the central x-y slice over one screw rotation.

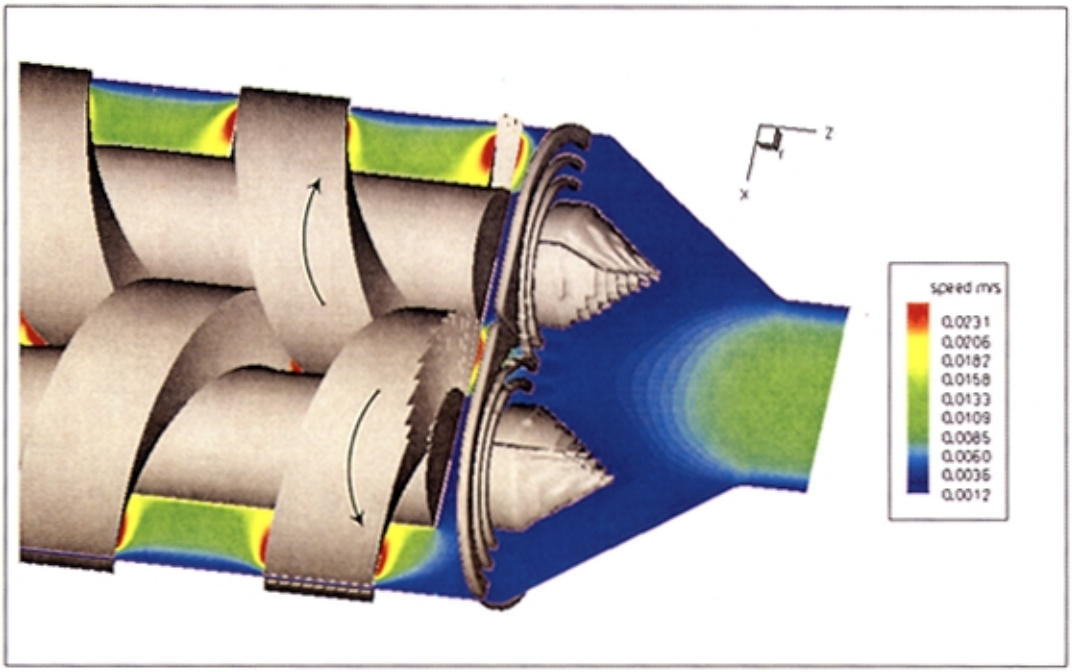

Figure 12. *Z*-velocity contours of the soap-plodder showing pressure plate and cone geometry.

chambers is primarily shear flow. The time evolution of F is shown for a central x-y plane in Figure 11b. The presence of elongational flows in the C-chambers, as well as the gaps, is seen clearly. The LEP was designed to deliver a high pumping efficiency at minimal shear degradation of the product, which is normally caused by the strain experienced by a fluid element while passing through a process equipment. This benefit of LEP can be assessed by extending the above analysis to estimate the total shear/elongational strain experienced by all the fluid elements while passing through the prevailing flow fields under given throughput/pressure gradient conditions, which is an activity we are planning for the future.

Another important task was to simulate an operating assembly LEP fitted with a concentric pressure plate (Chokappa et al., 1997) followed by a convergent cone and an extrusion die at the discharge end of the extruder. The geometry is shown in Figure 7 and Figure 12. The pressure plate with concentric rings was defined within the FC framework as $\Omega_{\text{body}}(t)$ by assigning the velocity field $\bar{u}(\bar{x}) = 0$ for cells lying within the plate. (Note that the feed hopper has not been included in our simulation, although it would not be very difficult to do so in the FC framework.) In addition, a more realistic non-Newtonian model (Herschel Bulkley) was used to describe the fluid rheology.

$$\begin{aligned} \tau_{ij} &= -2\mu\left(S_{ij}\right)^n \pm \tau_0 \quad & \tau_{ij} > \tau_0 \\ S_{ij} &= 0 & \tau_{ij} < \tau_0 \end{aligned} \tag{14}$$

where τ_0 is the yield stress and n is the power law index.

We simulated the plodder with a fairly coarse mesh (682,500 mesh elements). However, this exercise did bring out the feasibility to simulate efficiently an extremely complex piece of equipment with minimal effort spent on geometry creation and meshing, to obtain interesting insights into the plodder operation. Such a task would be inconceivable using the regular mesh deformation and reconstruction approach. In Figure 12 we have shown the contours of the speed values along the x-z plane. The throughput obtained from the simulated extruder was 1.15 tons per min at a RPM of 2. The throughput obtained in the factory was 2 tons per min. The lower throughput obtained in the simulations was due to the relatively larger clearance gaps specified in the geometry of our illustrative simulation exercise. As discussed earlier, larger leakage flow resulting from these clearance gaps do reduce the pumping efficiency of the plodder. The outflow from the extruder also shows pulsations. These pulsations could be picked up in the transient simulation of the extruder. The outflow velocity as a function of time for a screw

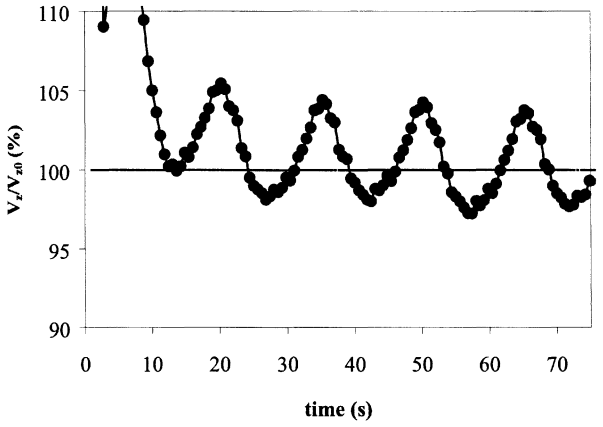

Figure 13. Oscillations in outflow from an intermeshed counter-rotating twin-screw extruder.

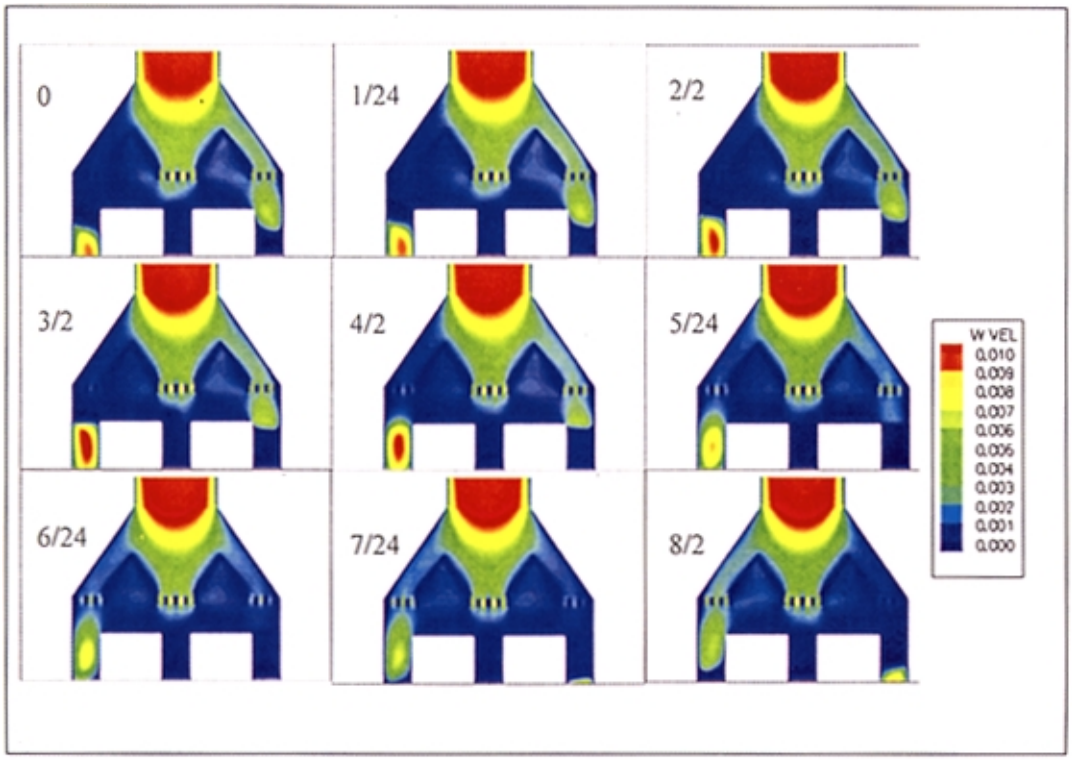

Figure 14. Sequence of *Z*-velocity contours over a half blade rotation showing the alternate discharging of the screws.

The time is shown as fraction of time for one screw revolution.

RPM = 2 has been plotted in Figure 13. The pulsations are clearly seen in the outflow with a time interval equal to half the rotation time for one screw ~15 s. They occur due to the alternating discharge of the contents of the C-chambers formed by the two screws. This is shown very nicely in Figure 14, where we have plotted the Z-velocity contours in the outlet region of the extruder as a function of time. The snapshots are shown over a period of a 1/3 rotation. The time shown in the figure is a fraction of the time for one screw rotation. The alternating discharge from the two screws can be seen clearly, where, at time $t = 0$, the discharge is from the right screw, while, at $t = 1/3$ revolution, the left screw starts discharging and reaches a maximum at $t = 1/2$ revolution. The crest in the pulsations occurs when any one screw is discharging at the maximum level, and the trough occurs when there is no discharge from both ends (*c.f.* $t = 6/24$).

Conclusion

In conclusion we have demonstrated the use of the "Forced Cell" method for simulating flow of complex fluids in very complex equipment.

A generalized algorithm for the FC method was developed and the method was successfully validated for the case of a single-screw extruder and a Newtonian fluid, by comparing results with those obtained using conventional techniques. The effect of the "rough surface" that comes about due to the partial coverage of a cell by a moving body was isolated and its effect on the velocity components and pressure were studied separately. It was shown that the forced cell approach gives very good agreement with the conventional approach. The presence of the rough surface in the case of the forced cell approach does not appear to significantly influence the velocity components or the pressure field for the Newtonian rheology studies. In fact we expect the agreement to be even better for pseudoplastic rheologies, as commonly encountered in the processing of soaps, detergents, plastics, and so on. Such materials, when trapped inside the rough edges, would experience very low shear and, hence, act like a solid mass tending to smooth out the rough surface. Having established its validity, the applicability and power of the FC method was demonstrated by simulating the complex 3-D flow in a commonly encountered processing equipment with multiple moving parts viz. an intermeshed counter-rotating twin screw extruder. Although no comparisons of CPU time are available, we expect that, in addition to the geometry generation and meshing time being considerably lower, the FC implementation would also afford significant savings in the computational time, as compared to the conventional techniques employing mesh deformation and regeneration. More importantly, the relevant geometric parameters (such as flight pitch, angle, radius, and so on, for the case of the extruder) can be varied by simply modifying values in the analytical expressions used to define them, thus making it possible to automate the design optimization. Despite the inaccuracies that might arise out of the non-body fitted mesh, the method can definitely be used to efficiently simulate process equipment to get a maiden-cut on the optimal design parameters. The more computationally intensive methods may then be used optionally to get a further refinement on the design.

Literature Cited

Avalosse, T., Y. Rubin, and L. Fondin, "Non-Isothermal Modeling of Co-rotating and Contra-rotating Twin Screw Extruders," *J. of Reinforced Plastics and Composites*, **21**(5), 419 (2002).

Chokappa, D. K., and V. M. Naik, "Process for the Manufacture of Soap Bars and Apparatus Therefor," Patent WO95/21907, PCT EP95/00317 (1995).

Chokappa, D. K., V. M. Naik, and A. Saxena, "Pressure Plate," Patent WO97/20915, PCT EP96/05379 (1997).

Duchanoy, C., and T. Jongen, "Efficient Simulation of Liquid/Solid Flows With High Solids Fraction in Complex Geometries," *Comput. and Fluids*, **32**, 1453 (2003).

Glowinski, R., T. W. Pan, and J. Periaux, "A Fictitious Domain Method for Dirichlet Problem and Applications," *Comp. Methods App. Mech. Eng.*, **111**, 283 (1994).

Gramann, P. J., A. C. Rios, and T. A. Osswald, "Comparative Study of Mixing in Twin Screw Extruders," *ANTEC*, **108** (1995).

Hirt, C. W., A. A. Amsden, and J. L. Cook, "An Arbitrary Lagrangian-Eulerian Computing Method for all Flow Speeds," *J. Comp. Phys.*, **14**, 227 (1974).

Ishikawa, T., S. I. Kihara, and K. Funatsu, "3-D Non-Isothermal Flow Field Analysis and Mixing Performance Evaluation of Kneading Blocks in a Co-Rotating Twin Screw Extruder," *Polym. Eng. Sci.*, **41**(5), 840 (2001).

Janssen, L. P. B. M., L. P. H. R. M. Mulders, and J. M. Smith, "Model for Output From Pump Zone of Double-Screw Processor or Extruder," *Plast. Polym.*, **43**, 93 (1975).

Janssen, L. P. B. M., *Twin Screw Extrusion*, Elsevier, Amsterdam (1978).

Jongen, T., "Simulation of Free-Surface Flows Induced by Partially Immersed Moving Body: Validation," *AIChE J.*, **46**(11), 2140 (2000).

Li, Tao, and I. Manas-Zloczower, "Flow-Field Analysis of an Intermeshing Counter Rotating Twin-Screw Extruder," *Poly. Eng. Sci.*, **34**(7), 551 (1994) .

Middleman, S., *Fundamentals of Polymer Processing*, McGraw-Hill, New York (1977).

Patankar, S. V., *Numerical Heat Transfer and Fluid Flow*, McGraw-Hill, New York (1980).

Patankar, S. V., and D. B. Spalding, "A Calculation Procedure for Heat, Mass and Momentum Transfer in Three-Dimensional Parabolic Flows," *Int. J. Heat Mass Transfer*, **15**, 1787 (1972).

Rowell, H. S., and D. Finlayson, "Screw Viscosity Pumps," *Engineering*, **126**, 249 (1928).

Rhie, C. M., and W. L. Chow, "Numerical Study of the Turbulent Flow. Past an Airfoil with Trailing Edge Separation," *AIAA J.*, **21**, 1527 (1983).

Rios, A. C., P. J. Gramann, and T. A. Osswald, "Comparative Study of Mixing in Corotating Twin Screw Extruders Using Computer Simulations" *Adv. in Poly. Tech.*, **17**(2), 107 (1998).

Shon, E., D. Chang, and J. L. White, "A Comparative Study of Residence Time Distributions in a Kneader, Continuous Mixer, and Modular Intermeshing Co-Rotating and Counter-Rotating Twin Screw Extruders," *Int. Polymer Processing.*, **14**, 44 (1999).

Shyy, W., H. S. Udaykumar, M. M. Rao, and R. W. Smith, *Computational Fluid Dynamics with Moving Boundaries*, Taylor and Francis, London (1996).

Singh, P., D. D. Joseph, T. I. Hesla, R. Glowinski, and T. W. Pan, "A Distributed Lagrange Multiplier/Fictitious Domain Method for Viscoelastic Particulate Flows," *J. Non-Newtonian Fluid Mech.*, **91**, 165 (2000).

Speur, J. A., H. Mavridis, J. Vlachopoulos, and L. P. B. M. Janssen, "Flow Patterns in the Calender Gap of a Counter Rotating Twin Screw Extruder," *Adv. Polym. Tech.*, **7**, 39 (1987).

Tanguy, P. A., F. Bertrand, R. Labrie, and E. B. La Fuente, "Numerical Modeling of the Mixing of Viscoplastic Slurries in a Helical Ribbon Screw Impeller," *TransI ChemE*, **74**, 499 (1996).

Van Doormal, J. P., and G. D. Raithby, "Enhancements of the SIMPLE Method for Predicting Incompressible Fluid Flows," *Num. Heat Transfer*, **7**, 147 (1984).

White, J. L., *Intermeshing Counter-Rotating Twin Screw Extrusion Technology*, Twin Screw Extrusion, Hanser Verlag, Berlin (1991).

Wilson, M. P., S. C. Generalis, All-Malaika, and D. P. Bruce, "Flow Field Analysis of some Mixing Element Regions within a Closely Intermeshing, Co-Rotating Twin Screw Extruder," *ICHEME Sym., Ser.*, **140**, 237 (1995).

Yang, H. H., and I. Manas-Zloczower, "Flow Field Analysis of Kneading Disc Region in a Co-Rotating Twin Screw Extruder," *Poly. Eng. Sci.*, **32**(19), 1411 (1992).

Ye, T., R. Mittal, H. S. Udaykumar, and W. Shyy, "An Accurate Cartesian Grid Method for Viscous Incompressible Flows with Complex Immersed Boundaries," *J. Comp. Physics*, **156**, 209 (1999).

Manuscript received Sept. 5, 2002, revision received Jan. 23, 2003, and final revision received Feb. 19, 2003.